Uncoupling the hydrolysis of lipid-linked oligosaccharide from the oligosaccharyl transfer reaction by point mutations in yeast oligosaccharyltransferase

Received for publication, June 29, 2020, and in revised form, September 12, 2020 Published, Papers in Press, September 16, 2020, DOI 10.1074/jbc.RA120.015013

Takahiro Yamasaki and Daisuke Kohda*

From the Division of Structural Biology, Medical Institute of Bioregulation, Kyushu University, Fukuoka, Japan

Edited by Gerald W. Hart

Oligosaccharyltransferase (OST) is responsible for the first step in the *N*-linked glycosylation, transferring an oligosaccharide chain onto asparagine residues to create glycoproteins. In the absence of an acceptor asparagine, OST hydrolyzes the oligosaccharide donor, releasing free *N*-glycans (FNGs) into the lumen of the endoplasmic reticulum (ER). Here, we established a purification method for mutated OSTs using a high-affinity epitope tag attached to the catalytic subunit Stt3, from yeast cells co-expressing the WT OST to support growth. The purified OST protein with mutations is useful for wide-ranging biochemical experiments. We assessed the effects of mutations in the Stt3 subunit on the two enzymatic activities *in vitro*, as well as their effects on the *N*-glycan attachment and FNG content levels in yeast cells. We found that mutations in the first D*X*D motif increased the FNG generation activity relative to the oligosaccharyl transfer activity, both *in vitro* and *in vivo*, whereas mutations in the DK motif had the opposite effect; the decoupling of the two activities may facilitate future deconvolution of the reaction mechanism. The isolation of the mutated OSTs also enabled us to identify different enzymatic properties in OST complexes containing either the Ost3 or Ost6 subunit and to find a 15-residue peptide as a better-quality substrate than shorter peptides. This toolbox of mutants, substrates, and methods will be useful for investigations of the molecular basis and physiological roles of the OST enzymes in yeast and other organisms.

N-Glycosylation refers to the covalent attachment of an oligosaccharide chain on asparagine residues in proteins and is one of the most important post-translational protein modifications (1–3). The *N*-glycosylation consensus, Asn-*X*-Ser/Thr (where *X* is not Pro), is the sequon, and the *N*-oligosaccharide chain attached to a protein is the *N*-glycan. The oligosaccharide donors are lipid-linked oligosaccharides (LLOs) (4). The oligosaccharide portion of LLO is transferred to the side-chain carboxamide group of asparagine residues in the sequon by the action of oligosaccharyltransferase (OST) (5). In higher eukaryotes, including the budding yeast *Saccharomyces cerevisiae*, the transfer of the 14-residue oligosaccharide chain, $Glc_3Man_9GlcNAc_2$, occurs on the luminal side of the endoplasmic reticulum (ER) membrane. Statistical studies revealed that two-thirds of the sequons are glycosylated (6). The proper selections of the sequons to be glycosylated or left unmodified are a prerequisite for the protein quality control in the ER and subsequent degradation in the cytosol (1, 2). Interestingly, oligosaccharide chains that are not attached to proteins reportedly accumulate inside the ER and the cytosol (7). The peptide:*N*-glycanase (PNGase), Png1, cleaves the *N*-glycans from misfolded glycoproteins in the cytosol. The PNGase-derived "free" *N*-glycans (FNGs) account for 95% of the total FNGs in the yeast cytosol (8). The yeast OST enzyme generates the remaining 5% of FNGs via LLO hydrolysis. The OST-derived FNGs are transported from the ER to the cytosol for degradation by a cytosol-vacuolar α-mannosidase, Ams1 (9, 10). The amounts of FNGs generated by OST can be measured using a *png1*Δ*ams1*Δ double-knockout strain, by suppressing the generation of the cytosol-originated FNGs (8). In contrast, most of the FNGs in the ER and the cytosol are attributed to the hydrolytic activity of OST in the ER lumen in mammalian cells (11).

The yeast OST enzyme is a membrane-embedded protein complex consisting of eight membrane-protein subunits in an equimolar ratio. Stt3, Wbp1, Swp1, Ost1, and Ost2 are essential gene products, whereas Ost3/Ost6, Ost4, and Ost5 are nonessential gene products (5). The Stt3 subunit has the catalytic site. In general, eukaryotic genomes encode multiple paralogous *stt3* genes (12). The homologous Stt3 proteins expressed from these paralogous genes generate different OST complexes. Except for *Caenorhabditis* species, the genomes from all sequenced metazoan organisms contain two STT3 genes (*STT3A* and *STT3B*). Plant genomes also encode two copies of STT3 genes (*STT3A* and *STT3B*) (13). In the phylum Protista, for example, the *Leishmania major* genome contains four *stt3* genes, *stt3A*, *stt3B*, *stt3C*, and *stt3D* (14). Despite their similar names, the human, plant, and protist genes lack direct orthologous relationships (13, 15). One important exception is fungi, including *S. cerevisiae*, with genomes encoding a single *stt3* gene. The human STT3B protein sequence is more similar to the yeast Stt3 protein sequence, suggesting that the human STT3A is a newcomer in evolution and the human STT3B is orthologous to the yeast Stt3 (15). In place of the single Stt3, the yeast genome encodes the two paralogous *ost3* and *ost6* genes, which generate two different OST forms containing either Ost3 or Ost6 (16). The ratio of the Ost3-containing to Ost6-containing OST complexes is 4:1 (8). Single deletions of either Ost3 or Ost6 resulted in moderate underglycosylation of proteins,

This article contains supporting information.

* For correspondence: Daisuke Kohda, kohda@bioreg.kyushu-u.ac.jp.

and the Ost3 and Ost6 double knockout led to severe underglycosylation in yeast cells (17). The Ost3 and Ost6 proteins have a thioredoxin fold in the N-terminal soluble domain, and the oxidoreductase activity was considered to suppress disulfide bond formation during the oligosaccharyl transfer reaction (18, 19). However, the *N*-glycosylation status was only affected to a limited extent by the disruption of the C*XX*C motifs in the Ost3 and Ost6 subunits, suggesting the importance of noncovalent interactions (19). The actual functions of the Ost3 and Ost6 subunits remain elusive.

In vivo mutagenesis studies of the individual subunits of yeast OST have been performed using the spotting plate assay. Switching from the WT OST to the mutated OST in cells is accomplished by the plasmid-shuffling method (20, 21) or the GAL1 promoter–switching method (22). The spotting plate assay is quite easy to execute, but its outcome is rather limited: a mutation is just classified into lethal, temperature-sensitive, or normal (*i.e.* nonconditional) growth phenotypes. Moreover, the different properties of the two OST complexes containing Ost3 or Ost6 *in vivo* could complicate the interpretation of the results obtained by the spotting plate assays. In some situations, enzymological studies using purified proteins with a defined subunit composition are preferred. However, the reconstitution of the OST complex *in vitro* using recombinant proteins has not been successful. Fortunately, the genetic manipulation of the yeast genome is straightforward. Previously, the 3×HA (hemagglutinin) epitope tag–encoding sequence was inserted at the 3′-ends of the *stt3* and *ost3* genes in the yeast genome, for immunopurification of the OST complexes and immunodetection of other subunits (20, 23) The tandem IgG-binding domain–encoding sequence of Protein A was added to the 3′-end of the *stt3* gene in the yeast genome for the same purpose (24). Subsequently, other types of epitope tag sequences (FLAG, 3×FLAG, and 1D4) were incorporated into the 3′-end of the *ost4* gene in the yeast genome, and the tagged OST complexes were affinity-purified to homogeneity for enzymatic investigation (8) and cryo-EM single-particle analyses (25–27). In the case of conditional mutations, the isolation of OST complexes containing such mutant proteins is possible, provided that the yeast strain can grow under permissive conditions. Yeast strains carrying the *stt3-4* and *stt3-6* (G520D), *stt3-5* (G520S), and *stt3-7* (S552P) alleles have temperature-sensitive phenotypes (24). These strains were grown at the permissive temperature of 23 °C, and the membrane fractions were prepared. In the membrane fractions, the OST complexes with these mutants showed very low oligosaccharyl transfer activities (24). In contrast, the introduction of lethal or very severe temperature-sensitive mutations into the Stt3 subunit is rather difficult, as the co-expression of the WT Stt3 subunit is necessary for cell culture. We must confirm that the OST preparation with the mutated Stt3 subunit is not contaminated with the native OST complex containing the WT Stt3 subunit.

In this study, we fused a new epitope tag to the 5′-end of the mutated *stt3* genes in expression plasmids. The epitope tag has a high affinity to a specific antibody (28) and enables the preparation of the mutated OST complex free from the native OST complex. In addition, the use of host yeast strains expressing either Ost3 or Ost6 permits the purification of the OST complexes with a defined subunit composition. We measured the oligosaccharyl transfer activity and the hydrolytic activity of LLO *in vitro*, using the Ost3-containing OST complexes carrying mutations in the catalytic Stt3 subunit. In parallel, we determined the *N*-glycosylation status of the glycoproteins and the amounts of FNGs generated by OST in yeast strains harboring the same *stt3* mutations. These detailed comparisons of the two activities of a series of mutations provided new insights into the *N*-glycosylation reactions *in vitro* and in living yeast cells.

Results

Affinity purification of the OST complexes containing mutations in the Stt3 subunit

The PA epitope tag sequence was inserted into the region encoding the N terminus of the Stt3 subunit via a 10-residue spacer sequence (Fig. 1*A*). The tagged Stt3 protein was expressed under the control of the constitutive glyceraldehyde-3-phosphate dehydrogenase (GPD) promoter from the expression plasmid, pPA-STT3. An Ost6-knockout strain (*ost6*Δ) was used as the host to prepare the Ost3-containing OST complex (referred to as OST[Ost3]). Deleterious effects caused by the absence of Ost6 were compensated by the extra expression of Ost3 from the pOST3 plasmid (27, 29). As mutational sites, we selected the two conserved short amino acid motifs, the first D*X*D motif from the two D*X*D motifs and the DK motif in the Stt3 subunit (Fig. 1*A*) (21, 30). These two short motifs are located close to the bound peptide substrate in the three-dimensional structure and involved in the recognition of the amino acid residues in or close to the sequon (Fig. 2). Glu^{45} is the first acidic residue of the D*X*D motif and is positioned to interact with the residue at position −1 of the sequon (27, 30), whereas Asp^{47} is the second acidic residue in the same motif and coordinates to the divalent metal ion in the catalytic center. Asp^{583}, Lys^{586}, and Met^{590} are the three signature amino acid residues that constitute the DK motif (21). Asp^{583} and Lys^{586} are directly and Met^{590} is indirectly involved in the formation of the Ser/Thr-binding pocket, which recognizes the hydroxy amino acid residue at position +2 in the sequon (31).

Even if a lethal mutation was introduced in the catalytic Stt3 subunit, the growth of the yeast host cells is supported by the native *stt3* gene in the genome. The E45K, D47A, and D583A mutations were lethal in the spotting plate assay (Fig. S1). The OST complexes containing Ost3 and the PA-tagged Stt3 subunit with a mutation (OST[Ost3, PA-Stt3(X)], where X denotes a mutation) were affinity-purified from digitonin-solubilized microsomal fractions and subjected to SDS-PAGE and CBB staining (Fig. 1*B*). No bands were present in the sample from the yeast cells transformed with the empty plasmid, indicating the absence of the native OST complex without the PA tag in the purified samples. The Wbp1 subunit contains two potential *N*-glycosylation sites. The total amount of Wbp1 was used to estimate the relative amounts of the mutation-bearing OST complexes to the WT OST complex with the PA tag (Fig. 1*B*). The quantification of the other subunits is less useful, due to diffused, adjacent, or high-mobility bands. The protein yields

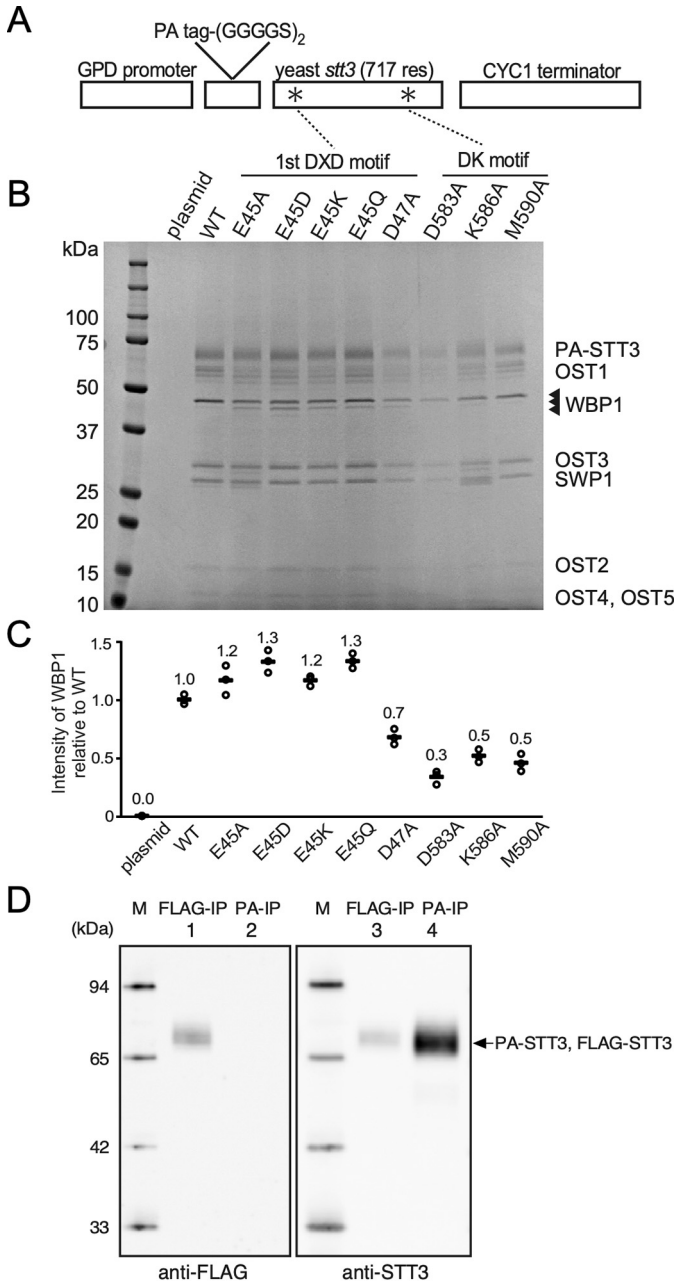

Figure 1. Purification of yeast OST complexes containing a point mutation in the Stt3 subunit. *A, schematic representation* of the gene construction for expression of the PA tag–fused Stt3 protein. The PA-tag sequence, GVAMPGAEDDVV, is inserted at the N terminus of the Stt3 protein via a 10-residue spacer sequence, $(GGGGS)_2$. Transcription is controlled by the GPD promoter and the CYC1 terminator. The *asterisks* indicate the positions of the mutations. *B*, CBB-stained gel image of the purified OST proteins, OST[Ost3, PA-Stt3(X)], where X denotes a point mutation. The *ost6*Δ-pOST3 yeast strain was used as the host to prepare the OST complex containing the Ost3 subunit alone. The *triangles* indicate the three bands corresponding to the non-, mono-, and diglycosylated forms of the Wbp1 subunit. *C*, protein yields based on the Wbp1 band intensities. The yield of the OST complex containing the WT Stt3 subunit with the PA tag is set to 1. *D*, check WT Stt3 incorporation into the OST preparation. Immunoprecipitated samples with the anti-FLAG tag antibody (*FLAG-IP*) and the anti-PA tag antibody (*PA-IP*) were analyzed by Western blotting. The WT Stt3 expressed from the chromosome was detected with the anti-FLAG antibody (*left*). The amounts of the Stt3 protein in the same sample volumes were measured with anti-STT3 antibody (*right*).

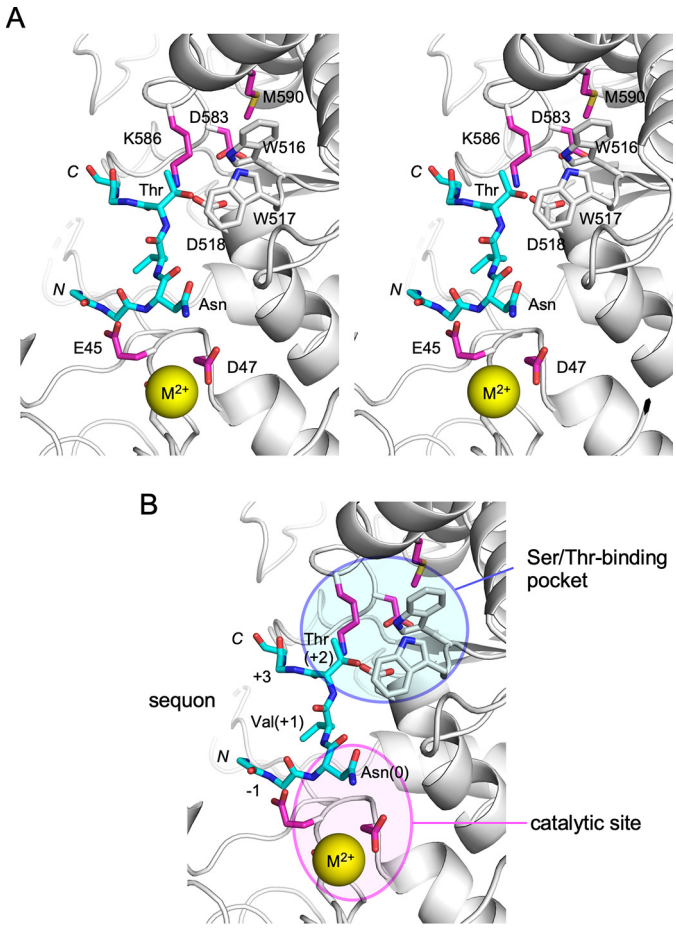

Figure 2. Point mutation sites in the three-dimensional structure of yeast OST. *A, stereoview* of the sequon-binding site of the yeast Stt3 subunit (Protein Data Bank entry 6EZN). The 7-residue peptide containing a sequon, Asn-Val-Thr, was adopted from the archaeal AglB-peptide complex (5GMY) after the superimposition of the AglB structure on the Stt3 structure and is shown in *cyan*. The side chains of the residues mutated in this study are *highlighted* in *magenta*. *B*, catalytic site around the bound divalent metal cation for the activation of the side-chain carboxamide group of the Asn residue at position 0 in the sequon. The Ser/Thr-binding pocket is formed by the residues in the WWDYG motif (Trp^{516}-Trp^{517}-Asp^{518}) and the DK motif (Asp^{583}-Lys^{586}-Met^{590}) for the recognition of the side-chain hydroxy group of the Ser/Thr residue at position +2 in the sequon.

were variable, but not lower than 30% of the WT OST with the PA tag (Fig. 1*C*). Finally, we checked the incorporation of the WT Stt3 protein expressed from the chromosome into the OST preparations, considering the oligomeric interactions between the OST molecules. We created a yeast strain carrying an *stt3* gene with a FLAG epitope tag–encoding sequence in the chromosome. The immunoprecipitated materials with the anti-FLAG antibody (FLAG-IP) and those with the anti-PA antibody (PA-IP) were analyzed by Western blotting (Fig. 1*D*). As a positive control experiment, the FLAG-IP sample was analyzed with the anti-FLAG antibody, indicating the presence of a single band (Fig. 1*D*, *lane 1*). In contrast, the PA-IP sample contained no detectable bands with the anti-FLAG antibody (*lane 2*), even though much larger amounts of the OST complex protein were loaded to the lanes of PA-IP (*lanes 2* and *4*) than those of FLAG-IP (*lanes 1* and *3*). We concluded that the genome-derived Stt3 was virtually absent in the OST preparations purified with the PA epitope tag.

Table 1
Substrate peptides used in this study

Peptide name	Amino acid sequence[a]	Preparative method
NVT9-tam	Ac-AAYNVTKRK(TAMRA) -COOH	Chemical synthesis[b]
tam-NVT9	(TAMRA)-GAYNVTAKR-COOH	Chemical synthesis
tam-NVT15	(TAMRA)-GAGGSYNVTKGAGGS-$CONH_2$	Chemical synthesis (32)
tam-NVT25	NH_2-GPC(TAMRA)-GAGGSGAGGSYNVTKGAGGSGAGGS-COOH	Protein expression and chemical modification[c]

[a] The *N*-glycosylation sequon is underlined. The peptide concentrations were determined by the absorbance at 555 nm, with an extinction coefficient of 90,000 M^{-1} cm^{-1}. The N-terminal α-amino group is either unmodified (NH_2-), modified with an acetyl group (Ac-), or modified with the TAMRA group (TAMRA-). The C-terminal α-carboxyl group is either unmodified (-COOH) or modified with an amide group (-$CONH_2$).
[b] TAMRA is attached to the side-chain ϵ-amino group of the C-terminal lysine residue.
[c] TAMRA is attached to the side-chain sulfhydryl group of the cysteine residue via the thiol-maleimide reaction.

Comparison of peptide substrates in the in vitro oligosaccharyl transfer assay

The oligosaccharyl transfer activities of the purified OST complexes were measured with LLO prepared from yeast cells as the oligosaccharide donor and various peptides containing the sequon Asn-Val-Thr as the oligosaccharide acceptor. The glycopeptide products were separated by normal-phase UPLC and quantified with in-line fluorescence detection of the carboxytetramethylrhodamine (TAMRA) dye attached to the peptide substrates. We designed four peptide substrates for the selection of a peptide substrate suitable for the oligosaccharyl transfer assay (Table 1). Kinetic parameters were determined using the OST[Ost3, PA-Stt3(WT)] complex. There were few differences in the maximal velocity (V_m), whereas considerable variations in the K_m were observed (Table 2 and Fig. S2). The 15-residue peptide substrate, tam-NVT15, had the smallest K_m value, indicating the highest affinity for the OST[Ost3] enzyme.

Effects of the position of the epitope tag

In addition to the OST complexes with the PA tag added to the Stt3 subunit, we prepared the OST complexes with the PA tag in the Ost4 subunit. The tag was inserted at the region encoding the C terminus of the *ost4* gene in the genome via a 15-residue spacer, $(GGGGS)_3$. To prepare the yeast OST complexes containing the Ost3 subunit alone, the *ost6*Δ knockout strain was used. The resulting strain and OST complex are referred to as *ost6*Δ *ost4*PA-pOST3 and OST[Ost3, Ost4-PA], respectively. The extra expression of Ost3 from the pOST3 plasmid reduces the deleterious effects caused by the absence of Ost6. In the same manner, we constructed the strain *ost3*Δ *ost4*PA-pOST6 and purified the OST[Ost6, Ost4-PA] complex. As for the Ost3-containing OST complex, two constructs bearing the PA tag in different subunits are available. We assessed the influence of the tag position (Fig. 3). The OST[Ost3, PA-Stt3] and OST[Ost3, Ost4-PA] complexes had the same specific activities for the oligosaccharyl transfer activity with the four different peptide substrates, indicating the negligible effects of the insertion and position of the PA tag. Additionally, the growth rates of the cells expressing the PA-tagged Ost4 and the PA-tagged Stt3 were the same as that of the WT cells (data not shown). These results indicate that the added PA tag has no detectable harmful effects, and the PA-tagged Ost4 and Stt3 proteins are fully functional *in vitro* and *in vivo*.

Effects of single-point mutations in the Stt3 subunit on the enzymatic activities in vitro

We measured the oligosaccharyl transfer activity of the OST complexes bearing mutations in the Stt3 subunit, OST[Ost3, PA-Stt3(X)], using the tam-NVT15 peptide as the oligosaccharide acceptor (Fig. 4*A*). The raw chromatographic data are presented in Fig. S3. The OST complex containing the lethal Stt3 (D47A) subunit had no detectable oligosaccharyl transfer activity, confirming the negligible WT OST complex contamination in the final preparations. A good correlation exists between the phenotypic level and the oligosaccharyl transfer activity (*inset* of Fig. 4*A*). In parallel, we measured the FNG generation activity (*i.e.* the hydrolytic activity of LLO) (Fig. 4*B* and Fig. S4). The mutated OST complexes were incubated with LLO in the absence of the peptide substrate. The released *N*-oligosaccharide chain was recovered by ethanol precipitation and fluorescently labeled by pyridylamination. Normal-phase UPLC was used to separate and quantify the 2-aminopyridine (2-AP)-labeled *N*-oligosaccharides. Note that the incubation time was longer (24 h) than that for the oligosaccharyl transfer assay (1 h), to compensate for the low hydrolytic activity. We checked the linearity of the reaction up to 30 h. There is no obvious correlation between the phenotypic level and the FNG generation activity (*inset* of Fig. 4*B*).

We then analyzed the correlation between the two *in vitro* activities (Fig. 4*C*). If the hydrolysis of LLO were a simple side reaction, then the two activities would show a linear relationship (the *dashed line* in Fig. 4*C*). However, the amino acid replacements of Glu^{45} increased, and the amino acid replacements of Lys^{586} and Met^{590} decreased, the FNG generation activity relative to the oligosaccharyl transfer activity. These results collectively indicate that the two activities can be uncoupled by single-point mutations in the catalytic Stt3 subunit.

Effects of single-point mutations in the Stt3 subunit on the N-glycosylation and FNG levels in yeast cells

The *N*-glycosylation statuses of the carboxypeptidase Y (CPY) protein and the Wbp1 subunit were measured to assess the *N*-glycosylation level *in vivo*. The CPY protein contains four potential *N*-glycosylation sites, and the Wbp1 subunit contains two potential sites, as mentioned above, resulting in five and three bands on the SDS-polyacrylamide gels, respectively (Fig. 5, *A* and *B*). Because the *N*-glycans of the two glycoproteins are dispensable for the growth of yeast cells, they are useful markers for monitoring the *N*-glycosylation level in yeast

Table 2
Enzyme kinetic parameters of the oligosaccharyl transfer reaction of the yeast OST complex for various peptide substrates

Peptide	K_m	V_m[a]
	μM	*fmol min*$^{-1}$
NVT9-tam	4.9 ± 0.3	2.9 ± 0.04
tam-NVT9	8.8 ± 1.3	4.1 ± 0.19
tam-NVT15	1.6 ± 0.2	3.3 ± 0.09
tam-NVT25	3.8 ± 0.3	3.5 ± 0.06

[a] In the presence of 2 μM LLO.

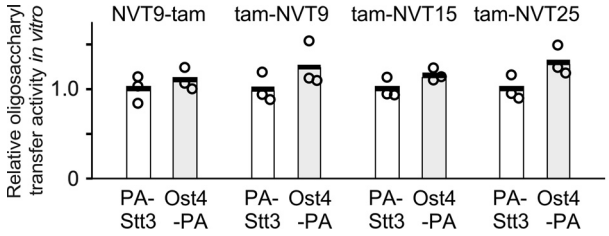

Figure 3. Effects of the epitope tag position on the oligosaccharyl transfer activity. The PA tag was attached to either the N terminus of the Stt3 subunit (PA-STT3) or the C terminus of the Ost4 subunit (Ost4-PA). The two OST complexes contain the Ost3 subunit alone. The four peptides in Table 2 were used as acceptor peptide substrates. The relative amounts of the PA-tagged OST complexes were estimated by fluorescent Western blotting of the Wbp1 subunit and used to normalize the activities. The activities of the OST with the tag in Stt3 were set to 1. The *bar heights* indicate the mean values of triplicate measurements. For statistical analysis, Welch's *t* test was applied, but no significant differences were detected ($p = 0.44$, 0.14, 0.26, and 0.073).

cells. Note that all of the *in vivo* experiments were conducted using yeast strains expressing both the Ost3 and Ost6 subunits from the genome (*stt3*Δ *png1*Δ *ams1*Δ-pSTT3(X)), and the OST complexes (OST[Ost3+Ost6, Stt3(X)]) did not contain any tags. The sequons in the two proteins were almost fully modified in yeast cells expressing OSTs containing the WT Stt3 or the Stt3(M590A) with normal growth phenotypes but were only partially modified in yeast cells expressing OSTs containing temperature-sensitive mutations, Stt3(E45A) and Stt3 (K586A). A good correlation exists between the oligosaccharyl transfer activities *in vitro* and the *N*-glycosylation statuses of CPY (Fig. 5*A*) and Wbp1 (Fig. 5*B*). We also measured the quantity of the total *N*-glycans attached to highly glycosylated mannoproteins expressed on the cell wall of yeast cells (Fig. S5*A*). The mannoproteins were recovered from the soluble fractions of cells after autoclave treatment, and the *N*-glycans were released from the mannoproteins by PNGase F digestion. In contrast to the *N*-glycans on CPY and Wbp1, the total *N*-glycan amounts remained the same in yeast cells expressing the mutated Stt3 subunit (Fig. S5*B*). This result indicates that the cell-wall integrity was maintained in yeast cells expressing these Stt3 mutants.

We then measured the amounts of FNG generated by OST in cells (Fig. 5*C* and Fig. S6). As expected, a good correlation exists between the FNG generation activity of the purified mutated OST enzymes and the amounts of FNG in the *stt3*Δ *png1*Δ *ams1*Δ-pSTT3(X) strains (Fig. 5*C*). In particular, yeast cells expressing Stt3(E45A) accumulated much more OST-derived FNG. This phenomenon could be caused by the increased supply of LLO. Thus, we measured the LLO contents in whole cells (Fig. S7). LLO was extracted from yeast cells and hydrolyzed to measure the amounts of released oligosaccharides. The Stt3(E45A) cells had a similar amount of LLO relative to the WT, indicating that the excessive supply of LLO is not the reason for the elevated FNG level in the Stt3(E45A)-expressing cells.

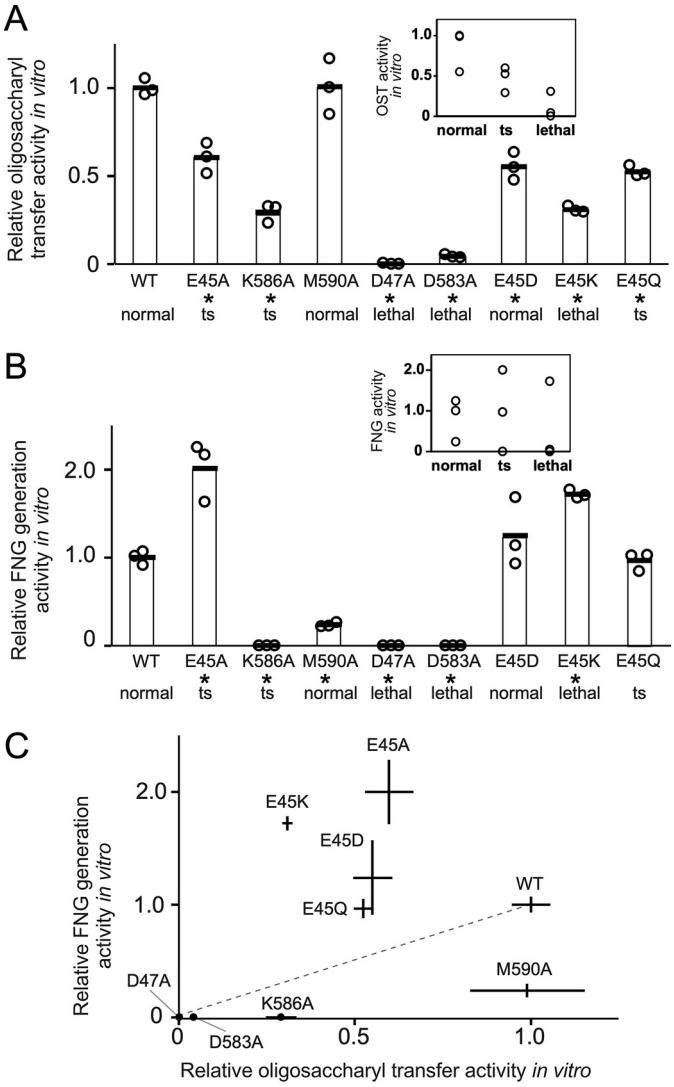

Figure 4. Oligosaccharyl transfer and FNG generation activities of the purified OST complexes containing a mutated Stt3 subunit. *A*, oligosaccharyl transfer activities of the purified OST[Ost3, PA-Stt3(X)] complexes, where X denotes a mutation. The peptide substrate was tam-NVT15. The primary UPLC chromatograms are shown in Fig. S3. *B*, free *N*-glycan generation activities of the purified OST[Ost3, PA-Stt3(X)] complexes. The primary UPLC chromatograms are shown in Fig. S4. In *A* and *B*, the relative amounts of the OST complexes bearing mutations were determined by CBB staining, as shown in Fig. 1*B*, and used to normalize the two activities. The *bar heights* indicate the mean values of triplicate measurements, and the *horizontal axes* in the *insets* represent the growth phenotypic level scored with a three-point ordinal scale. Welch's *t* test was applied between the WT and each mutant. *, $p < 0.05$. *C*, correlation plot between the oligosaccharyl transfer and FNG generation activities. *Error bars*, S.D. Data from *A* and *B*.

Different modes of action of the Ost3-containing and the Ost6-containing OST complexes in the in vitro assays

We assessed the effects of the exchange of the homologous Ost3 and Ost6 subunits (Fig. 6). The Ost3-containing OST complex, OST[Ost3, Ost4-PA], had higher oligosaccharyl transfer activity than the Ost6-containing OST complex, OST[Ost6,

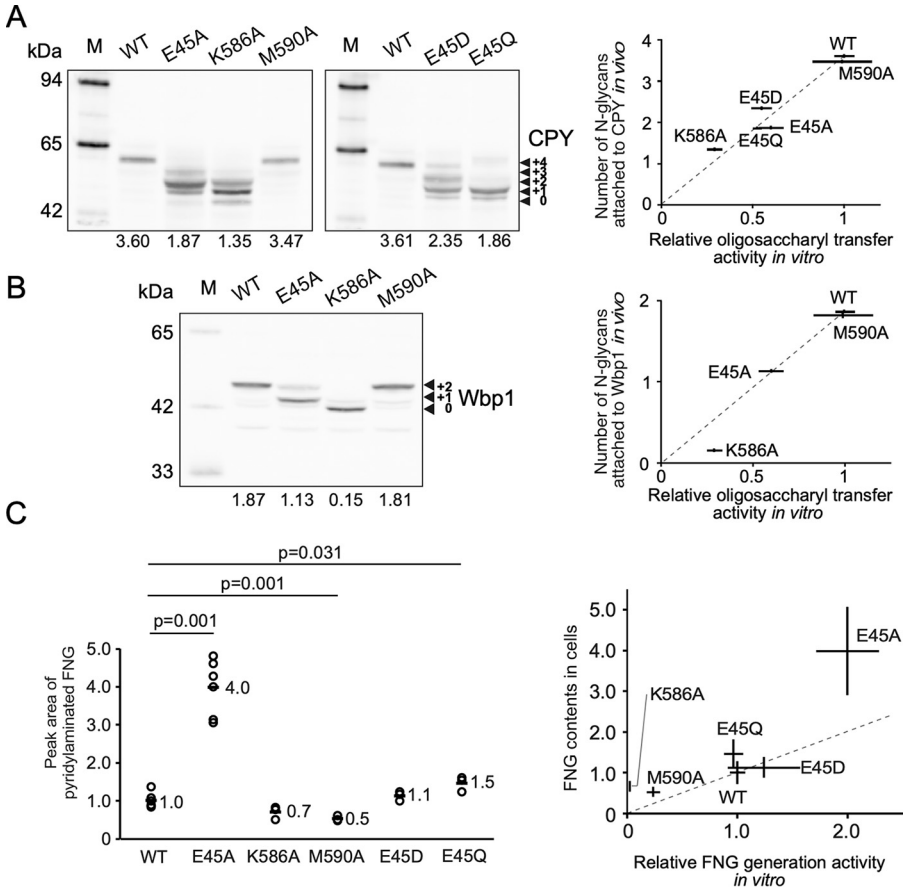

Figure 5. *N*-Glycosylation and FNG levels in mutated Stt3-expressing cells. *A*, *N*-glycosylation status of the CPY protein, determined by immunoblotting with the anti-CPY antibody. The values *below* the gel images are the average numbers of *N*-glycans attached to the CPY protein. The whole-cell lysates were obtained from the *stt3*Δ *png1*Δ *ams1*Δ-pSTT3(X) yeast strains, where X denotes a mutation. The *right panel* shows the correlation plot between the *N*-glycosylation levels (the number of *N*-glycans) of CPY in cells and the oligosaccharyl transfer activities of the purified OST[Ost3, PA-Stt3(X)], adopted from Fig. 4*A*. *B*, *N*-glycosylation status of the Wbp1 subunit of the OST complex, determined by immunoblotting with the anti-Wbp1 antibody. The values *below* the gel image are the average numbers of *N*-glycans attached to the Wbp1 protein. The whole-cell lysates were the same as those used in the CPY analyses. The *right panel* shows the correlation plot between the *N*-glycosylation levels (the number of *N*-glycans) of Wbp1 in cells and the oligosaccharyl transfer activities of the purified OST[Ost3, PA-Stt3(X)], adopted from Fig. 4*A*. *C*, contents of FNG in yeast strains, *stt3*Δ *png1*Δ *ams1*Δ-pSTT3(X), relative to that in the yeast strain harboring pSTT3(WT). The primary UPLC chromatograms are shown in Fig. S6. The *right panel* shows the correlation plot between the FNG contents in cells and the FNG generation activities of the purified OST[Ost3, PA-Stt3(X)], adopted from Fig. 4*B*. Welch's *t* test was applied for statistical analyses. In the correlation plots in *A*–*C*, the *horizontal* and *vertical error bars* represent the S.D. from three independent experiments, except for six independent experiments for WT in *A* and WT and E45A in *C*.

Ost4-PA], whereas the two OST complexes had similar FNG generation activities. We then tested the effects of the addition of the reducing agent DTT on the two activities because Ost3 and Ost6 are redox-related subunits. DTT had no effects on the oligosaccharyl transfer activity of the Ost3-containing OST complex, OST[Ost3, Ost4-PA], but enhanced the FNG generation activity more than 2-fold. In contrast, DTT had no effects on the two activities of the Ost6-containing OST complex, OST [Ost6, Ost4-PA]. These results suggest the unique roles of the Ost3 and Ost6 subunits in the recognition of a sequon-containing polypeptide chain and the generation of FNG in cells.

Discussion

Cell growth spotting assays have been used for mutational analyses of the yeast OST enzyme, based on the fact that *N*-glycosylation is essential for the survival and growth of yeast cells. The problem with these assays is that the dysfunction of the OST enzyme results in a simple growth phenotype, either lethal or temperature-sensitive. Moreover, the OST enzyme catalyzes the hydrolysis of the oligosaccharide donor, LLO, to release FNGs into the ER lumen. Although the physiological significance of the FNGs generated in the ER remains elusive, the functional modulation of the two activities in yeast cells could have diverse influences, eventually leading to an unpredictable growth phenotype. Thus, independent assessments of the two activities are desirable, using purified enzyme samples *in vitro*. In this study, we inserted the recently developed PA affinity tag into the region encoding the N terminus in the mutated *stt3* gene, under the control of the strong GPD promoter on the expression plasmid. The co-expression of the WT *stt3* gene from the yeast genome maintains the growth of yeast cells, even if the mutation is lethal. In previous studies, affinity tags were introduced to the C terminus of the Stt3 subunit (20, 21, 23, 24). Considering the membrane topology of the OST complex, the attachment to the N terminus would be better, because the N terminus is located on the opposite side of the ER membrane

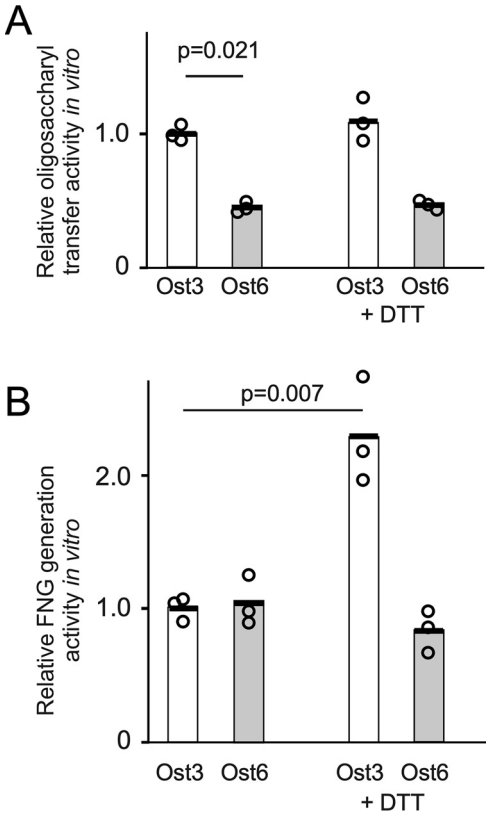

Figure 6. Effects of exchanging the Ost3 and Ost6 subunits on the enzymatic activities. *A*, *in vitro* oligosaccharyl transfer activities of the OST complexes containing either Ost3 or Ost6, in the absence and the presence of 5 mM DTT. The tam-NVT15 peptide was used in the oligosaccharyl transfer assay. *B*, same as *A*, but for FNG generation activities. In *A* and *B*, the PA tag was inserted at the C terminus of the Ost4 subunit. The relative amounts of the OST complexes containing either Ost3 or Ost6 were estimated by fluorescent Western blotting of the Wbp1 subunit and used to normalize the two activities. The activities of OST[Ost3, Ost4-PA] in the absence of DTT were set to 1. The *bar heights* indicate the mean values of triplicate measurements. Welch's *t* test was applied for statistical analyses.

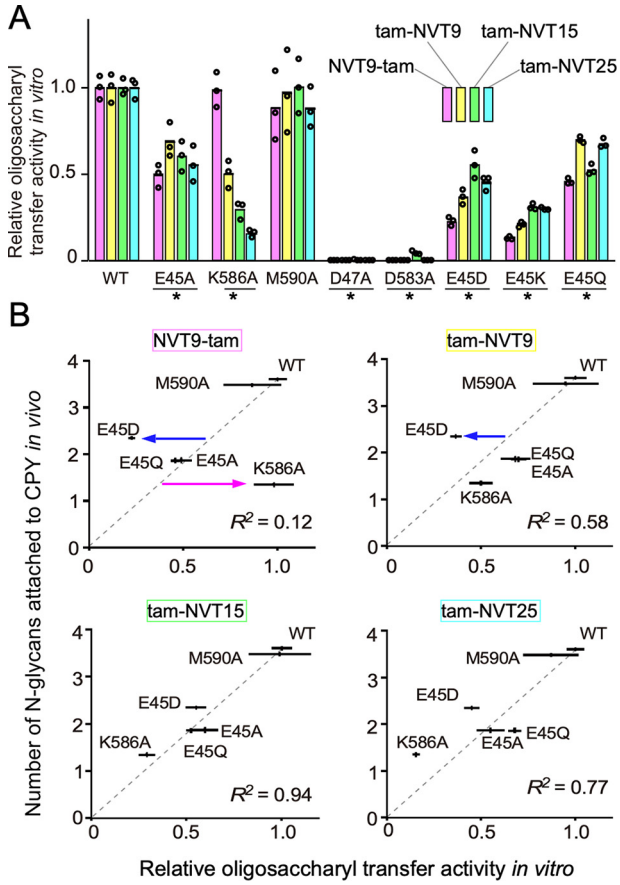

Figure 7. Correlation plots for the quality evaluation of peptide substrates. *A*, oligosaccharyl transfer activities of the OST[Ost3, PA-Stt3(X)] complexes, where *X* denotes a mutation, relative to those of the OST[Ost3, PA-Stt3(WT)] complex. The *bar heights* indicate the mean values of triplicate measurements. Welch's *t* test was applied between the WT and each mutant. *, $p < 0.05$. The four peptides listed in Table 2 were used as acceptor substrates. *B*, correlation plots. The *horizontal axis* represents the oligosaccharyl transfer activity *in vitro* taken from *A*, and the *vertical axis* represents the *N*-glycosylation status of CPY taken from Fig. 5*A*. Note that the plot with tam-NVT15 is identical to the correlation plot in the *inset* of Fig. 5*A*. The square of the correlation coefficient, R^2, is shown for each plot. The *dashed lines* simply connect the origin and the point corresponding to WT as a visual guide and are not the regression lines. The *magenta* and *blue horizontal arrows* indicate the outlier data points.

and is distant from the large luminal soluble domain, to avoid the risk of affecting the enzymatic activity. The 12-residue PA tag has a high affinity for the specific mAb, NZ-1 (28), and the binding of the PA tag (K_d = 0.49 nM) is 10–100-fold stronger than those of other frequently used tags, including the FLAG tag (K_d = 100 nM) (33) and the 1D4 tag (K_d = 20 nM) (34). The ultrahigh affinity withstands vigorous washing and hence ensures the minimal co-purification of the tagless OST complex containing the WT Stt3 subunit (Fig. 1). It is important to check the impacts of the tag attachment on the enzymatic activities. We compared the oligosaccharyl transfer activities between the two OST complexes containing the PA tag on the N terminus of the Stt3 subunit and that on the C terminus of the Ost4 subunit (Fig. 3). The results confirmed that the tag had no adverse effects on the enzymatic activity.

We selected amino acid residues in the first D*X*D motif (Glu^{45}–Asp^{47}) and the DK motif (Asp^{583}-Lys^{586}-Met^{590}) in the Stt3 sequence as mutational sites (21). These residues are positioned close to the peptide substrates in the bound state (Fig. 2) (26, 27). We purified the OST complexes containing the PA-tagged WT and mutated Stt3 subunits, OST[Ost3, PA-Stt3 (WT or X)], and measured their oligosaccharyl transfer and FNG generation activities in the presence and absence of the peptide substrates (Fig. 4). We also determined the growth phenotypes of the mutated yeast strains (*stt3*Δ-pSTT3(X)) (Fig. S1). Among them, we selected the Stt3 mutants with temperature-sensitive and normal growth phenotypes for further *in vivo* studies. The *stt3*Δ *png1*Δ *ams1*Δ-pSTT3(X) strains were cultured to stationary phase in YPD medium at a permissive temperature (30 °C) until the OD_{600} reached 10. We measured the *N*-glycosylation statuses of the CPY and Wbp1 glycoproteins *in vivo* (Fig. 5, *A* and *B*). CPY (carboxypeptidase Y) is a hydrolytic enzyme that catalyzes the release of amino acid residues from the C terminus of peptides in the vacuole. CPY is a soluble glycoprotein containing four *N*-glycosylation sites. Wbp1 is one of the eight subunits of the OST enzyme, with a single-spanning transmembrane helix and a large N-terminal soluble domain on the luminal side. The soluble domain contains two *N*-glycosylation sites. We also measured the total amounts of *N*-glycans attached to the cell-wall mannoproteins

(Fig. S5) and the FNG (Fig. 5*C*) and LLO (Fig. S7) contents in cells. Considering these results, we gained new insights as follows.

First, we discuss the different roles of the interchangeable Ost3 and Ost6 subunits. The previous *in vivo* studies demonstrated that the Ost3-containing and Ost6-containing OST complexes modified distinct repertoires of *N*-glycosylated proteins (18, 19). Here, we determined the different properties of the two isoforms of the OST complexes at the molecular level. The sequence identity (20%) and similarity (46%) are modest between Ost3 and Ost6 (17). The Ost3-containing OST complex had higher oligosaccharyl transfer activity than the Ost6-containing OST complex (Fig. 6*A*). The reducing agent DTT enhanced the FNG generation activity of the Ost3-containing OST complex more than 2-fold but had no effects on that of the Ost6-containing OST complex (Fig. 6*B*). Thus, the Ost3 and Ost6 subunits can affect the catalytic activity of Stt3 in unique and different manners, through a direct or indirect mechanism. Contrary to previous conceptions, a recent cell biological study has suggested that the oligosaccharyl transfer catalyzed by the yeast OST may not be a co-translational process coupled with the passage across the translocon channel (35), although the Ost3 and Ost6 subunits have been considered to interact with the translocon (26, 27). We expect that the different enzymatic properties of the Ost3-containing and Ost6-containing OST complexes *in vitro* will serve as a good starting point for future studies on the different roles of the Ost3/Ost6 subunits in yeast cells.

Second, the two activities of the OST enzyme can be uncoupled by single-point mutations in the Stt3 subunit. The replacements of Glu^{45} by Ala, Asp, Gln, and Lys enhanced the FNG generation activity relative to the oligosaccharyl transfer activity, and conversely, the replacements of Lys^{586} and Met^{590} by Ala suppressed the FNG generation activity (Fig. 4*C*). Lys^{586} and Met^{590} are distant from the catalytic center formed around the divalent metal ion (Fig. 2). Interestingly, the LLO hydrolytic activity can be manipulated by modulating the peptide binding mode remotely.

Third, under physiological conditions, the sequons are embedded in long, unfolded polypeptide chains in the co-translational mode or conformationally restricted yet flexible segments of folded polypeptides in the post-translational mode of the oligosaccharyl transfer reaction. In the oligosaccharyl transfer assays *in vitro*, short peptides up to 10 residues have conventionally been used. Thus, the use of peptides longer than 10 residues might be better in *in vitro* assays, to obtain a more realistic assessment of the OST enzyme activity inside the cells. We used the correlative relationship between the oligosaccharyl transfer activity *in vitro* and the *N*-glycosylation level of glycoproteins *in vivo* as an evaluating criterion. Fig. 7 shows the correlation plots for each of the four peptide substrates. Each point in the plots represents the data from a different mutation in the Stt3 subunit (Fig. 7*A*). The changes in the oligosaccharyl transfer activity *in vitro* by mutations are well-correlated with the changes in the *N*-glycosylation level in cells (*i.e.* the number of *N*-glycans attached to CPY) induced by mutation. With all data points considered, the 15-residue tam-NVT15 peptide shows the best correlation between the *in vitro* and *in vivo* activities (Fig. 7*B*). Therefore, we used this peptide in the subsequent oligosaccharyl transfer assays. A closer look at the data revealed some exceptions (the *magenta* and *blue horizontal arrows* in Fig. 7*B*). These exceptional preferences may be attributable to unwanted interactions of the positively charged, hydrophobic TAMRA dye with the mutation sites in the OST complex. This unexpected finding advises us to pay careful attention to the peptide substrate design.

Finally, the data in Figs. 4 and 5 are replotted from the standpoint of the individual mutants, for a more detailed discussion (Fig. 8). The five Stt3 mutants in Fig. 8 have a normal or temperature-sensitive phenotype. Even if the *N*-glycosylation level of CPY is retained to an extent of at least 30% of that in the WT cells, yeast cells can survive and grow at the permissive temperature, 30 °C. In the Stt3(E45Q) and Stt3(E45A) cells, the contents of FNG generated by OST increased 1.5- and 4-fold, respectively, suggesting that the high FNG levels formed in the ER lumen have no adverse effects on yeast cell growth. In Stt3 (M590A) cells, the content of FNG generated by OST decreased by 50%. The fact that the Stt3(M590A) strain has a normal growth phenotype indicates that a decrease in the FNG level in cells down to 50% is tolerable for yeast cell growth. These results are consistent with the previous report (8). The FNG levels as low as 10% of the WT cells in the *png1*Δ *ams1*Δ *ost3*Δ *ost6*Δ and the *png1*Δ *ams1*Δ *alg6*Δ strains sustained yeast cell growth.

Together, we did not find any vital functions of the FNG formed in the ER. However, it is tempting to speculate that the hydrolytic activity of LLO could be a second enzymatic activity preserved throughout eukaryotic evolution, during which the number of glycoproteins and the total number of modified sequons have expanded 10–20-fold (1). The FNGs generated in the ER might be necessary for yeast in special environments and other eukaryotic organisms even in normal growth environments and may serve as an organic osmolyte. In the case of the Gram-negative bacterium *Campylobacter*, the FNG generated by the bacterial OST in the periplasmic space is considered to play a role in balancing the osmotic pressure between the cytosol and extracellular environment (36, 37).

In conclusion, detailed comparisons of the two activities of a series of mutations in the Stt3 subunit *in vitro* and *in vivo* have provided new knowledge about the yeast OST enzyme: specifically, 1) the different properties between the Ost3- and Ost6-containing OST complexes, 2) the single-point mutations that change the relative activity of the LLO hydrolytic reaction to the oligosaccharyl transfer reaction, 3) the better design of peptide substrates, and 4) the dispensable function of FNG generated by OST under standard laboratory conditions. The uncoupling of the two activities by single-point mutations can offer useful insights into the generation mechanism and the physiological roles of the FNG generated in the ER. Previous *in vivo* knockout analyses of HEK293 and liver cells suggested that the human STT3B-containing OST complex generated FNG in cells, but the STT3A-containing OST complex did not (38). The mutations in the D*X*D motif and DK motif in the human STT3A/STT3B subunits will be helpful to confirm and investigate the functional differences between the two catalytic STT3 subunits in the human OST enzymes.

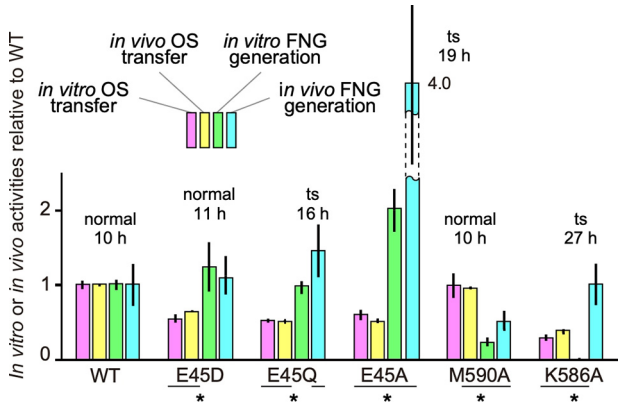

Figure 8. Comparison of the two *in vitro* and two *in vivo* activities for each of the OST complexes containing a mutated Stt3 subunit. The *in vitro* data were obtained with the purified OST[Ost3, PA-Stt3(X)] proteins, whereas the *in vivo* data were obtained with the yeast strains *stt3*Δ *png1*Δ *ams1*Δ-pSTT3(X), where X denotes a mutation. These data are redisplayed from Figs. 4 (*A* and *B*) and 5 (*A* and *C*) for a detailed comparison. Welch's *t* test was performed between the WT and each mutant. *, $p < 0.05$. The growth phenotype and the time required to reach OD_{600} 10 from 0.2 in the YPD medium at 30 °C are shown.

Experimental procedures

Reagents

2-AP, 5-fluoroorotic acid (5-FOA), digitonin, and borane-dimethylamine reagent were purchased from FujiFilm Wako Pure Chemical. The peptides used in the oligosaccharyl transfer assay were custom-synthesized (Hayashi Kasei, Osaka, Japan). A TAMRA group was introduced during the peptide synthesis to the N terminus and the side chain of a lysine residue. The mouse monoclonal anti-carboxypeptidase Y (CPY) antibody (10A5B5) was purchased from Abcam. The rabbit polyclonal anti-Wbp1 antibody and anti-Stt3 antibody were raised against a peptide fragment of yeast Wbp1 (residues 21–392 expressed as an N-terminally His-tagged protein) and that of yeast Stt3 (residues 485–718), respectively (21). The rabbit polyclonal anti-DDDDK-tag (anti-FLAG) antibody (PM020) was purchased from MBL. The peroxidase-conjugated anti-rabbit IgG antibody (NA934VS) was purchased from Amersham Biosciences ECL. The IRDye 800CW goat anti-rabbit IgG secondary antibody was purchased from LI-COR. The anti-FLAG M2–agarose (A2220) was purchased from Millipore. The XL-Western Marker (SP-2180) was purchased from Intégrale.

Yeast strains

Yeast strains used in this study are listed in Table 3. Gene disruption and tag insertion to the *stt3* gene were performed by the PCR-based technique (39). The N-terminal amino acid sequence fused to Stt3 is DYKDDDDK-$(GGGGS)_2$ (the FLAG epitope tag sequence followed by spacer sequence). The genomic *ost4* gene was C-terminally tagged with the PA epitope by two-step markerless gene replacement (40). The C-terminal amino acid sequence fused to Ost4 is $(GGGGS)_3$-GVAMPGAEDDVV (spacer sequence followed by the PA epitope). Correct tag integration was confirmed by PCR and DNA sequencing. For the selection of yeast strains containing pRS313-STT3(X) alone, a fresh colony of yeast strains, *stt3*Δ *png1*Δ *ams1*Δ containing pRS316-pSTT3 and pRS313-pSTT3(X) together, was inoculated on synthetic dropout medium (SD) containing 5-FOA and lacking L-histidine. Plates were incubated in an inverted position at 30 °C. The series of operations was repeated three times.

Plasmids

Plasmids used in this study are listed in Table 4. pRS313-STT3 was generated by the deletion of the 3×HA tag sequence (30 amino acid residues) from the pRS313-STT3-3HA plasmid constructed previously (21). The STT3 region is a 2,680-bp fragment containing the entire *stt3* gene (2,157 bp) plus 299 bp (native promoter) and 224 bp (native terminator) at the 5′- and 3′-ends, respectively. The pPA-STT3, pOST3, and pOST6 plasmids were constructed with a Gibson Assembly kit (New England Biolabs). The open reading frames of the *stt3*, *ost3,* and *ost6* genes were amplified using genomic DNA from the yeast strain BY4741 as the PCR template. For the construction of pPA-STT3, the GPD promoter, the yeast Stt3 sequence, and the CYC1 terminator were assembled into pRS313. The GPD promoter and the CYC1 terminator were derived from pAG416-GPD-ccdB as the PCR template. pAG416GPD-ccdB was a gift from Susan Lindquist (Addgene plasmid 14148; RRID:Addgene_14148). Then the DNA sequences corresponding to the PA tag, GVAMPGAEDDVV, and the spacer sequence, $(GGGGS)_2$, were inserted between the GPD promoter and the Stt3 sequence (Fig. 1*A*). For the construction of pOST3 and pOST6, the DNA sequences encoding Ost3 and Ost6 were inserted into the multiple cloning site of pAG416-GPD-ccdB. An inverse PCR-based site-directed mutagenesis kit (SMK-101, TOYOBO) was used to generate single-point mutations to generate pPA-STT3(X).

Plasmid shuffling and spotting plate assay

*Stt3*Δ cells bearing pRS316-STT3 encoding the WT *stt3* were transformed with p(RS313-)STT3(X), encoding the *stt3* gene containing a single-point mutation X. The transformants were grown in SD medium lacking L-histidine until the OD_{600} reached 1. Collected cells were diluted in a 5-fold series. Aliquots (3 μl) of each dilution were spotted onto SD plates lacking L-histidine and those lacking L-histidine supplemented with 5-FOA, at a final concentration of 1 mg ml^{-1}. After incubations at 25, 30, and 37 °C for 2 days, cell growth was assessed.

Extraction of LLO for in vitro assays

The yeast cells, strain BY4741, were grown in a 3-liter flask containing 1 liter of synthetic complete medium at 30 °C until the OD_{600} reached 10. Cells were collected and used for the extraction of LLO, as described previously (8). To determine the amount of LLO, we used the end point assay and acid-hydrolysis methods. The end point assay measures the maximum amount of the glycopeptide produced by OST in the presence of an excess of the peptide substrate. The acid hydrolysis method measures the oligosaccharide released from LLO by acid hydrolysis. The LLO was hydrolyzed using 20 mM hydrochloride in a 2-propanol/water mixture (1:1, v/v) at 100 °C for 30 min. After evaporation to dryness, the pellet was labeled with 2-AP (see below). The pyridylaminated oligosaccharides

Table 3
Yeast strains used in this study

Strain name	Genotype	Source	Purpose
BY4741	*MAT***a** *his3Δ1 leu2Δ0 met15Δ0 ura3Δ0*	Laboratory strain	Parental strain, source of LLO
*stt3*Δ-pSTT3	*MAT***a** *stt3*Δ::*KanMX* BY4741- pRS316-STT3	This study	Plasmid shuffling
*stt3*Δ *png1*Δ *ams1*Δ- pSTT3	MAT**a** *stt3*Δ::*KanMX png1*Δ::*HygMX ams1*Δ::*LEU2* BY4741- pRS316-STT3	This study	Plasmid shuffling
*stt3*Δ *png1*Δ *ams1*Δ- pSTT3/pSTT3(X)	MAT**a** *stt3*Δ::*KanMX png1*Δ::*HygMX ams1*Δ::*LEU2* BY4741- pRS316-STT3/pRS313-STT3(X)	This study	Plasmid shuffling
*stt3*Δ *png1*Δ *ams1*Δ- pSTT3(X)	MAT**a** *stt3*Δ::*KanMX png1*Δ::*HygMX ams1*Δ::*LEU2* BY4741- pRS313-STT3(X)	This study	Quantification of the glycosylation status of CPY and Wbp1, and the amounts of FNG, LLO, and mannoprotein *N*-glycans
*ost6*Δ-pOST3[a]	*MAT***a** *ost6*Δ::*LEU2* BY4741- pOST3	This study	Production of OST[Ost3, PA-Stt3(X)]
*ost6*Δ *ost4*PA-pOST3[a]	*MAT***a** *ost6*Δ::*LEU2 ost4*Δ::*ost4*-PA BY4741- pOST3	This study	Production of OST[Ost3, Ost4-PA]
*ost3*Δ*ost4*PA-pOST6[b]	*MAT***a** *ost3*Δ::*LEU2 ost4*Δ::*ost4*-PA BY4741- pOST6	This study	Production of OST[Ost6, Ost4-PA]
*ost6*Δ-FLAG*stt3*-pOST3[a]	*MAT***a** *ost6*Δ::*LEU2 stt3*Δ::*HygMX*-FLAG-*stt3* BY4741- pOST3	This study	Check contamination of mutated PA-Stt3 by WT FLAG-Stt3

[a]The extra expression of Ost3 from the pOST3 plasmid reduces the deleterious effects by the absence of Ost6.
[b]The extra expression of Ost6 from the pOST6 plasmid reduces the deleterious effects by the absence of Ost3.

Table 4
Plasmids used in this study

Plasmid name	Description	Source	Purpose
pRS316	CEN6/ARS4, URA3	BYP562, National BioResource Project Japan	Parental plasmid
pRS316-STT3	Described previously	Ref. 21	Expression of WT Stt3 under the native promoter
pRS313	CEN6/ARS4, HIS3	BYP559, National BioResource Project Japan	Parental plasmid, empty plasmid in Fig. 1 and Fig. S1
pRS313-STT3-3HA	Described previously	Ref. 21	Expression of WT Stt3 under the native promoter
pRS313-STT3	3×HA tag sequence was removed from pRS313-STT3-3HA	This study	Expression of WT and mutated Stt3 under the native promoter in plasmid shuffling experiments and other *in vivo* experiments
pSTT3(E45A)	pRS313-STT3(E45A)	This study	
pSTT3(E45D)	pRS313-STT3(E45D)	This study	
pSTT3(E45K)	pRS313-STT3(E45K)	This study	
pSTT3(E45Q)	pRS313-STT3(E45Q)	This study	
pSTT3(D47A)	pRS313-STT3(D47A)	This study	
pSTT3(D583A)	pRS313-STT3(D583A)	This study	
pSTT3(K586A)	pRS313-STT3(K586A)	This study	
pSTT3(M590A)	pRS313-STT3(M590A)	This study	
pAG416-GPD-ccdB	CEN6/ARS4, HIS3, GPD, CYC1, ccdB	14148, Addgene	Parental plasmid
pOST3	pAG416-GPD-OST3	This study	Compensate for the lack of Ost6
pOST6	pAG416-GPD-OST6	This study	Compensate for the lack of Ost3
pPA-STT3	pRS313-GPD-PA-spacer-STT3	This study	Expression of WT and mutated PA-Stt3 under the GPD promoter in the strain, *ost6*Δ-pOST3
pPA-STT3(E45A)	pRS313-GPD-PA-spacer-STT3(E45A)	This study	
pPA-STT3(E45D)	pRS313-GPD-PA-spacer-STT3(E45D)	This study	
pPA-STT3(E45K)	pRS313-GPD-PA-spacer-STT3(E45K)	This study	
pPA-STT3(E45Q)	pRS313-GPD-PA-spacer-STT3(E45Q)	This study	
pPA-STT3(D47A)	pRS313-GPD-PA-spacer-STT3(D47A)	This study	
pPA-STT3(D583A)	pRS313-GPD-PA-spacer-STT3(D583A)	This study	
pPA-STT3(K586A)	pRS313-GPD-PA-spacer-STT3(K586A)	This study	
pPA-STT3(K590A)	pRS313-GPD-PA-spacer-STT3(M590A)	This study	

were separated by Infinity 1290 UPLC (Agilent) with an AdvanceBio Glycan Mapping column (Agilent) and quantified by an in-line fluorescence detector. Solvent A was 100 mM ammonium acetate buffer, pH 4.5, and solvent B was 100% acetonitrile. The column was equilibrated with 20% solvent A at a flow rate of 0.5 ml min^{-1}. A linear gradient of solvent A was applied from 20 to 40% over 8.5 min. Typically, 10–20 nmol of LLO was obtained from 10 g of wet yeast cells from a 1-liter culture.

Affinity purification of the yeast OST complex bearing the PA tag

The OST complex was purified from yeast strains as described previously, with modifications (26). Yeast cells transformed with pPA-STT3(X) were grown in SD medium lacking appropriate nutrients (−Ura and −His). Recovered yeast cells were lysed with glass beads, and microsome fractions were collected by ultracentrifugation at 100,000 × *g*. The membrane pellets were resuspended and dissolved in 20 mM Tris-HCl buffer, pH 7.5, 1.5% digitonin, 0.5 M NaCl, 1 mM $MgCl_2$, 1 mM $MnCl_2$, 1 mM EDTA, 1 mM phenylmethylsulfonyl fluoride, protease inhibitor mixture (Roche Applied Science), and 10% (v/v) glycerol. After a 1-h incubation, the mixture was ultracentrifuged for 30 min at 100,000 × *g*, and the clarified supernatant was mixed with prewashed anti-PA tag antibody beads (Fujifilm Wako Pure Chemicals) at 4 °C overnight with gentle shaking. The affinity beads were collected by centrifugation and washed five times with 20 mM Tris-HCl buffer, pH 7.5, 0.1% digitonin, 150 mM NaCl, 1 mM $MgCl_2$, and 1 mM $MnCl_2$. Finally, the OST complex was eluted with the same buffer containing 0.1 mg ml^{-1} PA-tag peptide (Fujifilm Wako Pure Chemicals). The eluted fractions were separated by SDS-PAGE using gradient gels (10–20%). Staining with CBB (Fig. 1) and fluorescence measurement after Western blotting (Figs. 3 and 6) were used for protein quantification. In the Western blotting,

proteins in gels were transferred to Immobilon-FL PVDF membranes (Millipore). Anti-Wbp1 antiserum was used as the primary antibody at a dilution of 1:5,000, and IRDye-labeled goat anti-rabbit IgG was used as the secondary antibody at a dilution of 1:25,000. The fluorescence of the IRDye was measured by an Odyssey (LI-COR) imaging system. Note that the PA-tag peptide was not removed from the final protein solutions. We confirmed that the PA-tag peptide did not influence the enzymatic activities.

Check contamination of the yeast OST preparation by the WT Stt3

Yeast cells (*ost6*Δ-FLAG*stt3*-pOST3) transformed with pPA-STT3(WT) were grown in SD medium lacking appropriate nutrients (−Ura and −His). The materials containing FLAG-Stt3(WT) were immunoprecipitated from yeast cells expressing the chromosomal *stt3* gene using anti-FLAG affinity gel. The materials absorbed were eluted with the SDS sample buffer. Separately, the OST complex containing PA-Stt3(WT) expressed from the plasmid was immunopurified from the same yeast cells as described above. The collected materials were separated on SDS-PAGE using gradient gels (10–20%). The proteins in the gels were transferred to Immobilon-P PVDF membranes (Millipore), probed with the indicated antibodies, and visualized by chemiluminescence with the Super-Signal West Femto Maximum Sensitivity Substrate (Thermo Fisher Scientific). The anti-FLAG antibody and anti-STT3 antiserum were used at dilutions of 1:5000 and 1:1000, respectively. The peroxidase-conjugated anti-rabbit IgG antibody was used at a dilution of 1:12,500. The chemiluminescent images were recorded with an LAS-3000 multicolor image analyzer (Fuji Photo Film).

Oligosaccharyl transfer assay

The oligosaccharyl transfer assay was performed using the fluorescent peptide substrate method (32, 41). The reaction mixture (total 10 μl) contained 1 μM yeast LLO, 5 μM substrate peptide, and 1–5 nM purified WT or mutated OST protein, in 20 mM Tris-HCl buffer, pH 7.5, 5 mM $MnCl_2$, 5 mM $MgCl_2$, and 0.1% (v/v) Triton X-100. The substrate peptides were labeled with a fluorescent dye, TAMRA, for detection (Table 1). The reaction mixture was incubated for 1 h at 30 °C. The reaction was stopped by the addition of 2 μl of 60 mM EDTA-NaOH, pH 8.0. The reaction products were separated by Infinity 1290 UPLC (Agilent) with an AdvanceBio Glycan Mapping column and quantified by an in-line fluorescence detector. Solvent A was 100 mM ammonium acetate buffer, pH 4.5, and solvent B was 100% acetonitrile. The column was equilibrated with 25% solvent A at a flow rate of 0.5 ml min^{-1}. A linear gradient of solvent A was applied from 25 to 57% over 8.5 min. Kinetic parameters for peptide substrates were determined by nonlinear least-squares fitting of the initial rates in the presence of 2 μM LLO to the Michaelis–Menten equation, using the program Kaleidagraph version 4.5.1 (Synergy Software).

Pyridylamination

The reducing end of the oligosaccharides was derivatized with 2-AP as described previously, with some modifications (10). The dried oligosaccharides were incubated with 20 μl of 2-AP in acetic acid at 80 °C for 1 h. After the reaction, the mixture was incubated with 20 μl of dimethylamine borane reagent in acetic acid at 80 °C for 30 min. The excess 2-AP was removed using a MonoFas silica gel spin column (GL Sciences). The spin column was washed with water and then preequilibrated twice with 800 μl of 100% acetonitrile before use. The sample solution was mixed with 460 μl of 100% acetonitrile and loaded onto the spin column. The column was washed twice with 800 μl of 95% (v/v) acetonitrile. Water was added to the column to elute the fluorescently labeled oligosaccharides.

FNG generation assay

The purified OST complex was incubated with 1 μM LLO for 24 h at 30 °C in a 100-μl reaction solution, containing 20 mM Tris-HCl, pH 7.5, 5 mM $MnCl_2$, 5 mM $MgCl_2$, and 0.1% (v/v) Triton X-100. The incubation time was longer (24 h) than that for the oligosaccharyl transfer assay (1 h) to compensate for the low hydrolytic activity. The reaction was terminated by the addition of 1 μl of 0.5 M EDTA-NaOH, pH 8.0. A 300-μl aliquot of ethanol was added, and the reaction solution was incubated for 15 min at 4 °C. After centrifugation at 15,000 × *g* for 15 min, the supernatant was evaporated to dryness. The resultant pellet was labeled with 2-AP. The pyridylaminated oligosaccharides were separated by Infinity 1290 UPLC with an AdvanceBio Glycan Mapping column and quantified by an in-line fluorescence detector. Solvent A was 100 mM ammonium acetate buffer, pH 4.5, and solvent B was 100% acetonitrile. The column was equilibrated with 20% solvent A at a flow rate of 0.5 ml min^{-1}. A linear gradient of solvent A was applied from 20 to 40% over 14 min.

Quantification of the total N-glycans from mannoproteins

The total *N*-glycans from mannoproteins were extracted from yeast strains as described previously, with modifications (8). The yeast strains, *stt3*Δ *png1*Δ *ams1*Δ- pSTT3(X), were grown in YPD medium (1% yeast extract, 2% peptone, and 2% glucose) at 30 °C until the OD_{600} reached 10. 10 OD_{600} units of cells were harvested and washed twice with 4 ml of water. The washed cell pellets were resuspended in 1 ml of 10 mM sodium citrate buffer, pH 6.0, and autoclaved for 2 h at 121 °C. After centrifugation at 15,000 × *g* for 5 min, the supernatant was incubated with 3 ml of ethanol on ice for 15 min. The solution was centrifuged at 7,500 × *g* for 15 min, and the pellet was dried and dissolved in 200 μl of 0.1 M ammonium bicarbonate containing 50 units of PNGase F (New England Biolabs). The solution was incubated for 16 h at 37 °C. After inactivation by heating for 5 min at 95 °C, ethanol was added to the reaction mixture at a final volume percentage of 75%. After centrifugation at 15,000 × *g* for 15 min, the supernatant was dried and labeled with 2-AP. The pyridylaminated *N*-glycans were separated by Infinity 1290 UPLC with an AdvanceBio Glycan Mapping column and quantified by an in-line fluorescence detector. Solvent A was 100 mM ammonium acetate buffer, pH

4.5, and solvent B was 100% acetonitrile. The column was equilibrated with 28% solvent A, at a flow rate of 0.5 ml min^{-1}. A linear gradient of solvent A was applied from 28 to 40.8% over 19 min.

Determination of the N-glycosylation status of glycoproteins

The *stt3*Δ *png1*Δ *ams1*Δ-pSTT3(X) strains were cultured in YPD medium at the permissive temperature (30 °C) until the OD_{600} reached 10. 10 OD_{600} units of cells were harvested and washed twice with 1 ml of water. The whole-cell lysate was prepared as described previously (42). After centrifugation at 15,000 × *g* for 2 min, 6-μl aliquots of the supernatants were subjected to SDS-PAGE using gradient gels (10–20%). SDS sample buffer (50 mM Tris-HCl, pH 6.8, 1% (w/v) SDS, 10% (w/v) glycerol, 0.025% (w/v) bromphenol blue, and 100 mM DTT) was used for protein denaturation. The proteins in the gels were transferred to Immobilon-P PVDF membranes (Millipore), probed with the indicated antibodies, and visualized by chemiluminescence with the SuperSignal West Femto Maximum Sensitivity Substrate (Thermo Fisher Scientific). The anti-CPY antibody and anti-Wbp1 antiserum were used at dilutions of 1:10,000 and 1:5,000, respectively. The peroxidase-conjugated anti-mouse and anti-rabbit IgG antibodies were used at a dilution of 1:12,500. The chemiluminescent images were recorded with an LAS-3000 multicolor image analyzer (Fuji Photo Film). The average numbers of *N*-glycans attached to the CPY and the Wbp1 glycoproteins were calculated.

Quantification of FNG in cells

FNGs were extracted from yeast cells as described previously, with modifications (8). Yeast strains, *stt3*Δ *png1*Δ *ams1*Δ-pSTT3(X), were cultured in YPD medium until the OD_{600} reached 10. 100 OD_{600} units of cells were harvested and washed with PBS. The washed cells were resuspended in 1 ml of lysis buffer (20 mM Tri-HCl, pH 7.5, 10 mM EDTA), and then 3 ml of ice-cold ethanol was added. The solution was vortexed for 10 s and cooled on ice for 5 min, and this procedure was repeated three times. The homogenate was centrifuged at 7,500 × *g* for 15 min, and the supernatant was recovered and evaporated to dryness. The dried soluble oligosaccharide fraction was desalted on a column packed with AG 501-X8 ion-exchange resin (Bio-Rad) and then on an InertSep GC column (GL Sciences). After elution, the dried pellets were labeled with 2-AP. The pyridylaminated FNGs were separated by Infinity 1290 UPLC with an AdvanceBio Glycan Mapping column and quantified by an in-line fluorescence detector. Solvent A was 100 mM ammonium acetate buffer, pH 4.5, and solvent B was 100% acetonitrile. The column was equilibrated with 20% solvent A at a flow rate of 0.5 ml min^{-1}. A linear gradient of solvent A was applied from 20 to 40% over 25 min.

Quantification of LLO in cells

The yeast strains, *stt3*Δ *png1*Δ *ams1*Δ-pSTT3(X), were grown in YPD medium at 30 °C until the OD_{600} reached 10. 100 OD_{600} units were harvested and washed twice with 4 ml of water. The extraction and acid hydrolysis of LLO were performed as described above. After evaporation to dryness, the pellet was labeled with 2-AP. The pyridylaminated oligosaccharides were separated by Infinity 1290 UPLC with an AdvanceBio Glycan Mapping column and quantified by an in-line fluorescence detector. Solvent A was 100 mM ammonium acetate buffer, pH 4.5, and solvent B was 100% acetonitrile. The column was equilibrated with 20% solvent A at a flow rate of 0.5 ml min^{-1}. A linear gradient of solvent A was applied from 20 to 40% over 8.5 min.

Model building of the yeast OST-peptide complex

The three-dimensional structure model of the yeast OST-peptide complex was constructed, based on the cryo-EM structures of the yeast OST protein (Protein Data Bank entry 6EZN) by reference to the *Archaeoglobus fulgidus* AglB-peptide complex (5GMY). AglB is a single-subunit OST enzyme in the archaeal domain. The figures were generated with the PyMOL program, version 2.3.2 (Schrödinger, LLC).

Statistical analysis

The significance of differences in values was assessed by two-sided Welch's *t* test.

Data availability

All data relevant to this work are contained within the article or available upon request.

Acknowledgments—We thank Prof. Takashi Ito (Kyushu University) for the gift of yeast strains. The DNA sequencing service was provided by the Laboratory for Research Support at the Medical Institute of Bioregulation, Kyushu University.

Author contributions—T. Y. and D. K. conceptualization; T. Y. data curation; T. Y. formal analysis; T. Y. and D. K. validation; T. Y. investigation; T. Y. and D. K. visualization; T. Y. methodology; T. Y. and D. K. writing-original draft; T. Y. and D. K. writing-review and editing; D. K. supervision; D. K. funding acquisition; D. K. project administration.

Funding and additional information—This work was supported by Japan Society for the Promotion of Science KAKENHI Grants JP24370047, JP26119001, and JP26119002 (to D. K.)

Conflict of interest—The authors declare that they have no conflicts of interest with the contents of this article.

Abbreviations—The abbreviations used are: LLO, lipid-linked oligosaccharide; 2-AP, 2-aminopyridine; CBB, Coomassie Brilliant Blue; CPY, carboxypeptidase Y; ER, endoplasmic reticulum; FNG, free *N*-glycan; 5-FOA, 5-fluoroorotic acid; GPD, glyceraldehyde 3-phosphate dehydrogenase; OD, optical density; OST, oligosaccharyltransferase; PA, a high-affinity tag; PNGase, peptide:*N*-glycanase; TAMRA, 5(6)-carboxytetramethylrhodamine; tam, TAMRA; UPLC, ultraperformance liquid chromatography; PVDF polyvinylidene difluoride.

References

1. Cherepanova, N., Shrimal, S., and Gilmore, R. (2016) *N*-Linked glycosylation and homeostasis of the endoplasmic reticulum. *Curr. Opin. Cell Biol.* **41,** 57–65 CrossRef Medline
2. Aebi, M. (2013) *N*-Linked protein glycosylation in the ER. *Biochim. Biophys. Acta* **1833,** 2430–2437 CrossRef Medline
3. Breitling, J., and Aebi, M. (2013) *N*-Linked protein glycosylation in the endoplasmic reticulum. *Cold Spring Harb. Perspect. Biol.* **5,** a013359 CrossRef Medline
4. Hartley, M. D., and Imperiali, B. (2012) At the membrane frontier: a prospectus on the remarkable evolutionary conservation of polyprenols and polyprenyl-phosphates. *Arch. Biochem. Biophys.* **517,** 83–97 CrossRef Medline
5. Kohda, D. (2018) Structural basis of protein Asn-glycosylation by oligosaccharyltransferases. *Adv. Exp. Med. Biol.* **1104,** 171–199 CrossRef Medline
6. Apweiler, R., Hermjakob, H., and Sharon, N. (1999) On the frequency of protein glycosylation, as deduced from analysis of the SWISS-PROT database. *Biochim. Biophys. Acta* **1473,** 4–8 CrossRef Medline
7. Chantret, I., and Moore, S. E. H. (2008) Free oligosaccharide regulation during mammalian protein *N*-glycosylation. *Glycobiology* **18,** 210–224 CrossRef Medline
8. Harada, Y., Buser, R., Ngwa, E. M., Hirayama, H., Aebi, M., and Suzuki, T. (2013) Eukaryotic oligosaccharyltransferase generates free oligosaccharides during *N*-glycosylation. *J. Biol. Chem.* **288,** 32673–32684 CrossRef Medline
9. Chantret, I., Kodali, V. P., Lahmouich, C., Harvey, D. J., and Moore, S. E. H. (2011) Endoplasmic reticulum-associated degradation (ERAD) and free oligosaccharide generation in *Saccharomyces cerevisiae*. *J. Biol. Chem.* **286,** 41786–41800 CrossRef Medline
10. Hirayama, H., Seino, J., Kitajima, T., Jigami, Y., and Suzuki, T. (2010) Free oligosaccharides to monitor glycoprotein endoplasmic reticulum-associated degradation in *Saccharomyces cerevisiae*. *J. Biol. Chem.* **285,** 12390–12404 CrossRef Medline
11. Harada, Y., Masahara-Negishi, Y., and Suzuki, T. (2015) Cytosolic-free oligosaccharides are predominantly generated by the degradation of dolichol-linked oligosaccharides in mammalian cells. *Glycobiology* **25,** 1196–1205 CrossRef Medline
12. Kelleher, D. J., Karaoglu, D., Mandon, E. C., and Gilmore, R. (2003) Oligosaccharyltransferase isoforms that contain different catalytic STT3 subunits have distinct enzymatic properties. *Mol. Cell.* **12,** 101–111 CrossRef Medline
13. Niu, G., Shao, Z., Liu, C., Chen, T., Jiao, Q., and Hong, Z. (2020) Comparative and evolutionary analyses of the divergence of plant oligosaccharyltransferase STT3 isoforms. *FEBS Open Bio.* **10,** 468–483 CrossRef Medline
14. Nasab, F. P., Schulz, B. L., Gamarro, F., Parodi, A. J., and Aebi, M. (2008) All in one: *Leishmania major* STT3 proteins substitute for the whole oligosaccharyltransferase complex in *Saccharomyces cerevisiae*. *Mol. Biol. Cell* **19,** 3758–3768 CrossRef Medline
15. Kelleher, D. J., and Gilmore, R. (2006) An evolving view of the eukaryotic oligosaccharyltransferase. *Glycobiology* **16,** 47R–462 CrossRef Medline
16. Schwarz, M., Knauer, R., and Lehle, L. (2005) Yeast oligosaccharyltransferase consists of two functionally distinct sub-complexes, specified by either the Ost3p or Ost6p subunit. *FEBS Lett.* **579,** 6564–6568 CrossRef Medline
17. Knauer, R., and Lehle, L. (1999) The oligosaccharyltransferase complex from *Saccharomyces cerevisiae*: isolation of the OST6 gene, its synthetic interaction with OST3, and analysis of the native complex. *J. Biol. Chem.* **274,** 17249–17256 CrossRef Medline
18. Poljak, K., Selevsek, N., Ngwa, E., Grossmann, J., Losfeld, M. E., and Aebi, M. (2018) Quantitative profiling of *N*-linked glycosylation machinery in yeast *Saccharomyces cerevisiae*. *Mol. Cell. Proteomics* **17,** 18–30 CrossRef Medline
19. Schulz, B. L., Stirnimann, C. U., Grimshaw, J. P. A., Brozzo, M. S., Fritsch, F., Mohorko, E., Capitani, G., Glockshuber, R., Grütter, M. G., and Aebi, M. (2009) Oxidoreductase activity of oligosaccharyltransferase subunits Ost3p and Ost6p defines site-specific glycosylation efficiency. *Proc. Natl. Acad. Sci. U. S. A.* **106,** 11061–11066 CrossRef Medline
20. Li, G., Yan, Q., Nita-Lazar, A., Haltiwanger, R. S., and Lennarz, W. J. (2005) Studies on the *N*-glycosylation of the subunits of oligosaccharyl transferase in *Saccharomyces cerevisiae*. *J. Biol. Chem.* **280,** 1864–1871 CrossRef Medline
21. Igura, M., Maita, N., Kamishikiryo, J., Yamada, M., Obita, T., Maenaka, K., and Kohda, D. (2008) Structure-guided identification of a new catalytic motif of oligosaccharyltransferase. *EMBO J.* **27,** 234–243 CrossRef Medline
22. Hese, K., Otto, C., Routier, F. H., and Lehle, L. (2009) The yeast oligosaccharyltransferase complex can be replaced by STT3 from *Leishmania major*. *Glycobiology* **19,** 160–171 CrossRef Medline
23. Karaoglu, D., Kelleher, D. J., and Gilmore, R. (1997) The highly conserved Stt3 protein is a subunit of the yeast oligosaccharyltransferase and forms a subcomplex with Ost3p and Ost4p. *J. Biol. Chem.* **272,** 32513–32520 CrossRef Medline
24. Spirig, U., Glavas, M., Bodmer, D., Reiss, G., Burda, P., Lippuner, V., Te Heesen, S., and Aebi, M. (1997) The STT3 protein is a component of the yeast oligosaccharyltransferase complex. *Mol. Gen. Genet.* **256,** 628–637 CrossRef Medline
25. Chavan, M., Chen, Z., Li, G., Schindelin, H., Lennarz, W. J., and Li, H. (2006) Dimeric organization of the yeast oligosaccharyl transferase complex. *Proc. Natl. Acad. Sci. U. S. A.* **103,** 8947–8952 CrossRef Medline
26. Bai, L., Wang, T., Zhao, G., Kovach, A., and Li, H. (2018) The atomic structure of a eukaryotic oligosaccharyltransferase complex. *Nature* **555,** 328–333 CrossRef Medline
27. Wild, R., Kowal, J., Eyring, J., Ngwa, E. M., Aebi, M., and Locher, K. P. (2018) Structure of the yeast oligosaccharyltransferase complex gives insight into eukaryotic *N*-glycosylation. *Science* **359,** 545–550 CrossRef Medline
28. Fujii, Y., Kaneko, M., Neyazaki, M., Nogi, T., Kato, Y., and Takagi, J. (2014) PA tag: a versatile protein tagging system using a super high affinity antibody against a dodecapeptide derived from human podoplanin. *Protein Expr. Purif.* **95,** 240–247 CrossRef Medline
29. Spirig, U., Bodmer, D., Wacker, M., Burda, P., and Aebi, M. (2005) The 3.4-kDa Ost4 protein is required for the assembly of two distinct oligosaccharyltransferase complexes in yeast. *Glycobiology* **15,** 1396–1406 CrossRef Medline
30. Shrimal, S., and Gilmore, R. (2019) Oligosaccharyltransferase structures provide novel insight into the mechanism of asparagine-linked glycosylation in prokaryotic and eukaryotic cells. *Glycobiology* **29,** 288–297 CrossRef Medline
31. Matsumoto, S., Taguchi, Y., Shimada, A., Igura, M., and Kohda, D. (2017) Tethering an *N*-glycosylation sequon-containing peptide creates a catalytically competent oligosaccharyltransferase complex. *Biochemistry* **56,** 602–611 CrossRef Medline
32. Igura, M., and Kohda, D. (2011) Quantitative assessment of the preferences for the amino acid residues flanking archaeal *N*-linked glycosylation sites. *Glycobiology* **21,** 575–583 CrossRef Medline
33. Einhauer, A., and Jungbauer, A. (2001) Affinity of the monoclonal antibody M1 directed against the FLAG peptide. *J. Chromatogr. A* **921,** 25–30 CrossRef Medline
34. Locatelli-Hoops, S. C., Gorshkova, I., Gawrisch, K., and Yeliseev, A. A. (2013) Expression, surface immobilization, and characterization of functional recombinant cannabinoid receptor CB2. *Biochim. Biophys. Acta* **1834,** 2045–2056 CrossRef Medline
35. Shrimal, S., Cherepanova, N. A., Mandon, E. C., Venev, S. V., and Gilmore, R. (2019) Asparagine-linked glycosylation is not directly coupled to protein translocation across the endoplasmic reticulum in *Saccharomyces cerevisiae*. *Mol. Biol. Cell* **30,** 2626–2638 CrossRef Medline
36. Dwivedi, R., Nothaft, H., Reiz, B., Whittal, R. M., and Szymanski, C. M. (2013) Generation of free oligosaccharides from bacterial protein *N*-linked glycosylation systems. *Biopolymers* **99,** 772–783 CrossRef Medline
37. Nothaft, H., Liu, X., McNally, D. J., Li, J., and Szymanski, C. M. (2009) Study of free oligosaccharides derived from the bacterial *N*-glycosylation pathway. *Proc. Natl. Acad. Sci. U. S. A.* **106,** 15019–15024 CrossRef Medline
38. Lu, H., Fermaintt, C. S., Cherepanova, N. A., Gilmore, R., Yan, N., and Lehrman, M. A. (2018) Mammalian STT3A/B oligosaccharyltransferases

segregate *N*-glycosylation at the translocon from lipid-linked oligosaccharide hydrolysis. *Proc. Natl. Acad. Sci. U. S. A.* **115,** 9557–9562 CrossRef Medline

39. Longtine, M. S., McKenzie, A., Demarini, D. J., Shah, N. G., Wach, A., Brachat, A., Philippsen, P., and Pringle, J. R. (1998) Additional modules for versatile and economical PCR-based gene deletion and modification in *Saccharomyces cerevisiae*. *Yeast* **14,** 953–961 CrossRef Medline
40. Widlund, P. O., and Davis, T. N. (2005) A high-efficiency method to replace essential genes with mutant alleles in yeast. *Yeast* **22,** 769–774 CrossRef Medline
41. Yamasaki, T., and Kohda, D. (2019) A radioisotope-free oligosaccharyltransferase assay method. *Bio-Protocol* **9,** CrossRef
42. Kushnirov, V. V. (2000) Rapid and reliable protein extraction from yeast. *Yeast* **16,** 857–860 CrossRef Medline